Dynamic Image Segmentation System for Ultrasonic B-mode Image Based on its Multi-Scaled Feature Maps

Ken'ichi Fujimoto[†], Mio Musashi[‡], and Tetsuya Yoshinaga[†]

†Institute of Health Biosciences and ‡Graduate School of Health Sciences
The University of Tokushima
3-18-15, Kuramoto, Tokushima, Tokushima 770-8509, Japan
Email: {fujimoto | yosinaga}@medsci.tokushima-u.ac.jp, musashi@anan-nct.ac.jp

Abstract—We have developed a dynamic image segmentation system for a gray-level image. It consists of a multi-scaling system and a discrete-time coupled system of chaotic neurons. Since an ultrasonic B-mode image, which is a gray-level image, generally has speckle noise, ordinary our system does not work well for such an image. This paper describes improvement of ordinary our system based on feature maps of an ultrasonic B-mode image. We showed a result of dynamic image segmentation performed for an ultrasonic B-mode image using an improved system.

1. Introduction

Image segmentation is the first essential and important step in a computer-aided diagnosis support system for a medical image with gray-levels. The authors have developed a discrete-time coupled system of chaotic neurons [1] and a global inhibitor for dynamic image segmentation [2]. Moreover, it has been extended to dynamic gray-level image segmentation system [3] using a multi-scaling system [4]. Adequate setting of its local excitatory couplings and global inhibitory couplings gives a result that chaotic neurons can generate appropriate oscillatory responses formed by periodic points with high order of periods for dynamic image segmentation. However, our system [3] such that excitatory couplings are determined with multi-scaled pixel values does not work well for an ultrasonic B-mode image because of speckle noise.

This paper describes improvement of our system [3]. Concretely, we consider determination of excitatory couplings based on feature maps calculated with texture analysis for an ultrasonic B-mode image. We show a result of dynamic image segmentation performed for an ultrasonic B-mode image of a sponge under the water.

2. Dynamic Gray-Level Image Segmentation System

2.1. Coupled System of Chaotic Neurons

Our coupled system [2] for N-pixel image consists of a global inhibitor and N chaotic neurons that are arranged in a grid so that a chaotic neuron corresponds to a pixel in an input image. The dynamics of the ith chaotic neuron for $i = 1, 2, \ldots, N$ is described as

$$x_i(t + 1) = k_f x_i(t) + I_i + C_i \tag{1}$$

$$y_i(t + 1) = k_r y_i(t) - \alpha g(x_i(t) + y_i(t), 0) + a \tag{2}$$

where t denotes the discrete time. I_i stands for a direct current (DC) input and takes a non-negative value associated with the ith pixel value. C_i represents the sum of excitatory couplings from chaotic neurons in its neighborhood including itself and an inhibitory coupling from the global inhibitor; it is described as

$$C_i = \sum_{k \in L(i)} \frac{W}{M(i)} g(x_k + y_k, 0) - W g(z, 0.5) \tag{3}$$

where $L(i)$ denotes a set of chaotic neurons corresponding to pixels with similar gray-levels at the ith pixel and its four-neighborhood. $M(i)$ is the number of elements in $L(i)$. $g(\cdot, \cdot)$ denotes the output function of a chaotic neuron or the global inhibitor and is defined as

$$g(v, \theta) = \frac{1}{1 + \exp(-(v - \theta)/\varepsilon)}. \tag{4}$$

The dynamics of the global inhibitor is expressed as

$$z(t + 1) = \phi \left\{ g\left(\sum_{i=1}^{N} g(x_i(t) + y_i(t), W), 0 \right) - z(t) \right\}. \tag{5}$$

Under setting of adequate couplings, chaotic neurons can generate appropriate oscillatory responses formed by periodic points for dynamic image segmentation.

2.2. Determination of Excitatory Coupling

To apply our system [2] to a dynamic gray-level image segmentation, we have to give definitions of a DC-input and an excitatory coupling that correspond to I_i and $M(i)$, respectively. As an idea to solve them, we introduced an iterative multi-scaling system [4]. It is similar to the K-means method [5] and can perform degradation of a gray-level image, i.e., it produces a multi-scaled image. However, unlike the K-means method, it does not need the number and the initial arrangement of clusters as prior information; it can also compute the proximity of gray-levels between two pixels in a multi-scaled image, simultaneously.
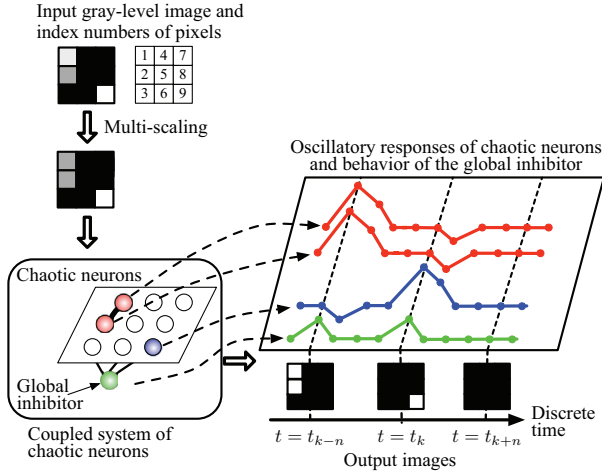
Figure 1: Dynamic gray-level image segmentation scheme.

(a) Whole image

(b) Partial image

Figure 2: Ultrasonic B-mode image of a sponge under the water and its (62×62)-pixel partial image trimmed at a region of the sponge.

We explain the multi-scaling algorithm [4]. Let $p_i(\tau)$ be the ith pixel value normalized in the range of $[0, 1]$ at the discrete time τ. Its updating rule is defined as
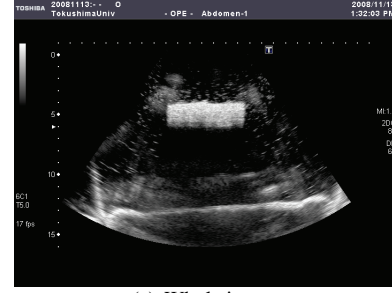
$$p_i(\tau + 1) = \begin{cases} 0 & \text{if } p_i(\tau) + \eta F_i(\tau) \leq 0 \\ p_i(\tau) + \eta F_i(\tau) & \text{if } 0 < p_i(\tau) + \eta F_i(\tau) < 1 \\ 1 & \text{if } p_i(\tau) + \eta F_i(\tau) \geq 1 \end{cases}$$

(6)

$$F_i(\tau) = \frac{\displaystyle\sum_{j \in \Delta_i(\tau)} \frac{p_j(\tau) - p_i(\tau)}{|p_j(\tau) - p_i(\tau)|} \exp\left(-\gamma |p_j(\tau) - p_i(\tau)|\right)}{S_i(\tau)}$$
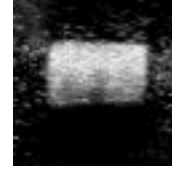
(7)

where the initial value $p_i(0)$ is given by the normalized gray-level of the ith pixel in an input image. $\Delta_i(\tau)$ denotes a set of pixels with similar values to $p_i(\tau)$. The sign $|\cdot|$ expresses the absolute value. $S_i(\tau)$ stands for the number of elements in the set $\Delta_i(\tau)$ and is counted based on the proximity level $q_{ij}(\tau)$ between the ith and jth pixel values at every iteration. Its updating is performed as

$$q_{ij}(\tau + 1) = \beta q_{ij}(\tau) + (1 - \beta)H\left(\exp\left(-\gamma |p_j(\tau) - p_i(\tau)|\right) - \psi\right)$$

(8)

where H denotes the Heaviside step function and returns zero or one if its argument value is negative or non-negative, respectively. η, γ, β, and ψ are positive parameters, and the each value except for γ is set as less than one. Therefore, the value of $q_{ij}(\tau)$ gradually converges to the return value of H, e.g., $q_{ij}(\tau + 1)$ approaches one when the values of $p_i(\tau)$ and $p_j(\tau)$ are close. Based on the values of $q_{ij}(\tau)$s, the values of $p_i(\tau)$s are also converged to several clusters. As the results, we obtain a multi-scaled image. Besides, according to the values of p_is and q_{ij}s after sufficient iteration, the value of I_i in Eq. (1) is associated with the value of p_i, and each coupling between two adjacent chaotic neurons is determined so that the ith and kth ($k \in L(i)$) chaotic neurons are coupled only if $q_{ik} = 1$.
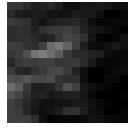
2.3. Dynamic Gray-Level Image Segmentation Scheme

The architecture of our coupled system and dynamic image segmentation scheme for a gray-level image with 3×3 pixels are illustrated in Fig. 1. The gray-level input image has two high-gray-level image regions: one is composed of two different gray-level pixels, which are the first and second pixels, and the other is the ninth pixel. As illustrated in Fig. 1, at first, multi-scaling for all pixel values is performed; consequently, similar pixel values become the same values, and the values of I_is and $M(i)$s are determined. In this case, the first and second chaotic neurons are coupled. The ith chaotic neuron with high I_i value can oscillate; and moreover, oscillatory responses of all adjacent chaotic neurons in $L(i)$ are synchronized in phase. When one or more chaotic neurons fire, the global inhibitor fires and inhibits the activity levels of all chaotic neurons at the next time. Therefore, isolated chaotic neurons fire separately. By associating the output value of each chaotic neuron with each pixel value every discrete time, segmented images are generated and are exhibited in time series.

3. Improvement of Our System

Since excitatory couplings are determined based on only a multi-scaled image of an input image in our ordinary system [3], the system cannot work for an ultrasonic B-mode image because of speckle noise. To improve our system, we investigated useful texture features of an ultrasonic B-mode image. As an example, let us consider a segmentation problem for an image of a sponge under the water shown in Fig. 2(a). In this study, to simplify the problem we dealt

Table 1: Typical values of the mean and skewness of pixel values at internal and peripheral regions of the sponge.

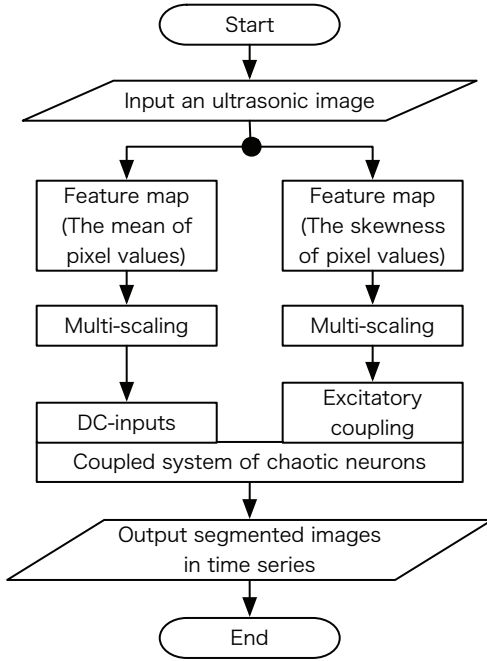|	Internal region	Peripheral region
Image		
Mean	168.59	18.963
Skewness	−0.35918	2.9248

Figure 3: Flowchart of processes in improved our system.

with not the whole image but its partial image trimmed at the region of the sponge shown in Fig. 2(b).

Through texture analysis for the partial image, we selected the mean and skewness of pixel values as features to separate the region of sponge from its peripheral region. Their typical values in the respective local regions are shown in Tab. 1. Besides, we also investigated the adequate size of windows to compute them. As the result, we determined the windows' size for computing the mean and skewness as 3×3 pixels and 15×15 pixels, respectively.

Based on the analyzed results, our ordinary system [3] was improved as illustrated in Fig. 3. At first, for an input image, we compute the mean and skewness in the respective windows throughout, i.e., two feature maps are created. Let f_i^{mean} and f_i^{skew} be the ith feature values in the feature maps on the mean and the skewness, respectively. Their values are multi-scaled based on the procedures de-
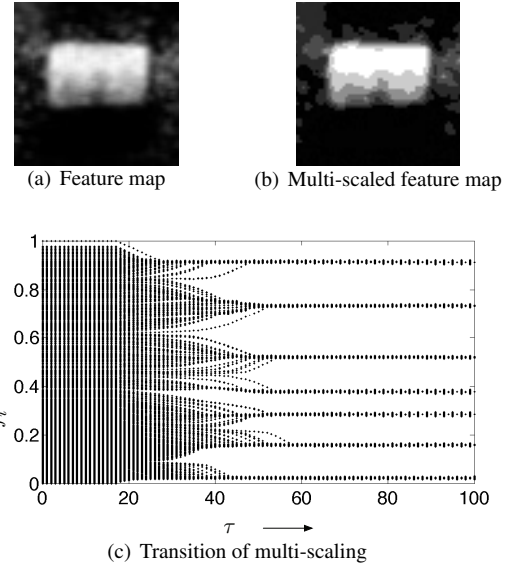

(a) Feature map (b) Multi-scaled feature map

(c) Transition of multi-scaling

Figure 4: Multi-scaling of a feature map on the mean of pixel values in respective 3×3 local regions.

scribed in Sec. 2.2. Note that f_i^{skew} is transformed as

$$f_i^{\mathrm{skew}} \leftarrow \min\left(1.0, \max\left(0, 2 * \left(0.5 - f_i^{\mathrm{skew}}\right)\right)\right) \quad (9)$$

before its multi-scaling. Using multi-scaled values, $\hat{f}_i^{\mathrm{mean}}$ and $\hat{f}_i^{\mathrm{skew}}$, in the respective feature maps, we defined as $I_i = 2\hat{f}_i^{\mathrm{mean}}$ and the value of $M(i)$ is the number of $\hat{f}_k^{\mathrm{skew}} \simeq 1, k \in L(i)$, respectively.

4. Experimental Results

For the input image shown in Fig. 2(b), according to the procedures described in Sec. 3, we created feature maps on the mean and skewness of pixel values as shown in Figs. 4(a) and 5(a), respectively. Subsequently, the respective feature maps were multi-scaled. Figures 4(c) and 5(c) show the transitions of their multi-scaling where the parameter values in Eqs. (6)–(8) were set as $\eta = 0.01$, $\gamma = 5$, $\beta = 0.1$, and $\psi = 0.5$. In each figure, its abscissa denotes the discrete time, and dots at every discrete time represent the distribution of normalized f_i^{mean} or f_i^{skew} in the range of $[0, 1]$. Although f_i^{mean}s and f_i^{skew}s were distributed throughout the range of $[0, 1]$ at $\tau = 0$, the distribution eventually converged to several clusters without the number and the initial arrangement of clusters as prior information. As the results, multi-scaled feature maps were obtained shown in Figs. 4(b) and 5(b).

We calculated as $I_i = 2\hat{f}_i^{\mathrm{mean}}$ where $\hat{f}_i^{\mathrm{mean}}$ is the ith pixel value with a real number in the image shown in Fig. 4(b). The value of $M(i)$ was also determined according to the values of $\hat{f}_k^{\mathrm{skew}}$, $k \in L(i)$, which are associated with the ith real pixel value in Fig. 5(b). Using our improved
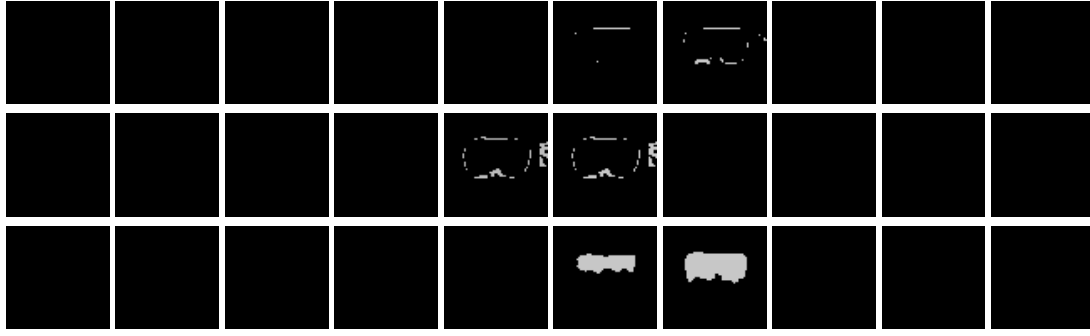
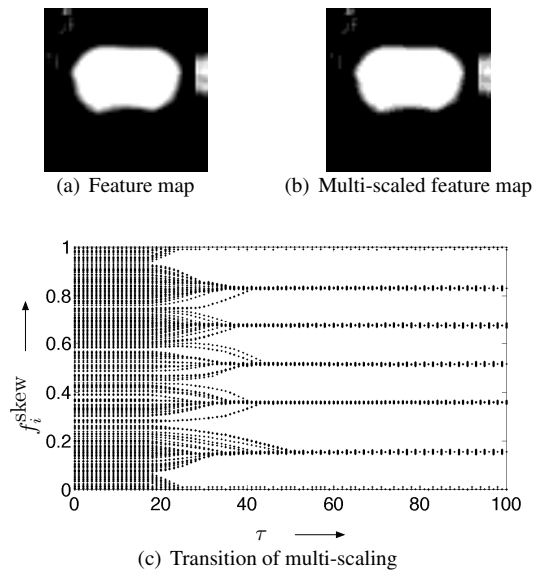Figure 6: Result of dynamic image segmentation performed for the ultrasonic B-mode image shown in Fig. 2(b).

(a) Feature map   (b) Multi-scaled feature map

(c) Transition of multi-scaling

Figure 5: Multi-scaling of a feature map on the skewness of pixel values in respective 15×15 local regions.

5. Concluding remarks

To avoid difficulty of segmentation due to speckle noise in an ultrasonic B-mode image, we improved our dynamic gray-level image segmentation system based on two multi-scaled feature maps of a input image. Each feature map was calculated by analyzing the texture of the input image and was multi-scaled using a multi-scaling system. The values of DC-inputs and excitatory couplings in our coupled system were determined based on the multi-scaled feature maps. For a partial image of an ultrasonic B-mode image, we demonstrated that our improved system worked not perfectly but acceptably. To more improve the segmenting performance of the proposed system in this study, we should design excitatory couplings in our coupled system elaborately in the future.

system, dynamic image segmentation for the gray-level image including speckle noise in Fig. 2(b) was performed. In the numerical experiment, we set the values of system parameters in Eqs. (1)–(5) as $k_f = 0.5$, $k_r = 0.885$, $\alpha = 4$, $a = 0.5$, $W = 15$, $\varepsilon = 0.1$, and $\phi = 0.8$; the initial values of the chaotic neurons and the global inhibitor were given randomly. Figure 6 shows a result of dynamic image segmentation performed, i.e., snapshot of output images every discrete time in steady state. The images sequentially appear from the top-left to the bottom-right in the figure. Moreover, their appearances in each line also start from the left. Now, to explain, let us the time that the top-left image outputs be zero. The outline of the sponge and its peripheral region were segmented at $t = 5, 6, 14, 15$, and an internal region of the sponge was segmented at $t = 25, 26$. Therefore, the result indicates that our improved system can be applicable to segment an ultrasonic B-mode image including speckle noise.

References

[1] K. Aihara, T. Takabe, and M. Toyoda, "Chaotic neural networks," *Phys. Lett. A*, vol.144, pp.333–340, 1990.

[2] K. Fujimoto, M. Musashi, and T. Yoshinaga, "Discrete-time dynamic image segmentation system," *Electron. Lett.*, vol.44, no.12, pp.727–729, 2008.

[3] K. Fujimoto, M. Musashi, and T. Yoshinaga, "Multi-Scaling of Gray Level Image and its Dynamic Image Segmentation Using Discrete-time Dynamical Systems," *IEICE Tech. Report*, 2009. (in press)

[4] L. Zhao, R.A. Furukawa, and A. C. P. L. F. Carvalho, "A network of coupled chaotic maps for adaptive multi-scale image segmentation," *Int. J. Neural Syst.*, vol.13, no.2, pp.131–139, 2003.

[5] J.A. Hartigan and M.A. Wong, "A K-means clustering algorithm," *Appl. Stat.*, vol.28, pp.100–108, 1979.